

Abstract

We present **PhasorFlow**, an open-source Python library introducing a computational paradigm operating on the S^1 unit circle. Inputs are encoded as complex phasors $z = e^{i\theta}$ on the N -Torus (\mathbb{T}^N). As computation proceeds via unitary wave interference gates, global norm is preserved while individual components drift into \mathbb{C}^N , allowing algorithms to natively leverage continuous geometric gradients for predictive learning. PhasorFlow provides three core contributions. First, we formalize the *Phasor Circuit* model (N unit circle threads, M gates) and introduce a 22-gate library covering Standard Unitary, Non-Linear, Neuro-morphic, and Encoding operations with full matrix algebra simulation. Second, we present the *Variational Phasor Circuit* (VPC), analogous to Variational Quantum Circuits (VQC), enabling optimization of continuous phase parameters for classical machine learning tasks. Third, we introduce the *Phasor Transformer*, replacing expensive QK^TV attention with a parameter-free, DFT-based token mixing layer inspired by FNet. We validate PhasorFlow on non-linear spatial classification, time-series prediction, financial volatility detection, and neuromorphic tasks including neural binding and oscillatory associative memory. Our results establish unit circle computing as a deterministic, lightweight, and mathematically principled alternative to classical neural networks and quantum circuits. It operates on classical hardware while sharing quantum mechanics' unitary foundations. PhasorFlow is available at <https://github.com/mindverse-computing/phasorflow>.

Keywords: unit circle computing, phasor circuits, variational circuits, Fourier transform, transformer, brain-computer interface, oscillatory computing

PhasorFlow: A Python Library for Unit Circle Based Computing

Dibakar Sigdel^{1*}, Namuna Panday¹
¹ Mindverse Computing LLC, WA, USA

March 18, 2026

1 Introduction

The landscape of computation has historically been defined by the mathematical structures upon which data is represented and transformed. Classical digital computers operate on discrete bits—points on a zero-dimensional manifold $\{0, 1\}$. Quantum computers leverage qubits, which reside in the complex projective space $\mathbb{C}\mathbb{P}^1$, enabling true quantum superposition and non-local entanglement through unitary operations on exponentially scaling Hilbert spaces [1]. Between these extremes lies a rich hierarchy of computational manifolds that remain largely unexplored in the context of programmable classical computing frameworks.

We refer to this hierarchy as the *Geometric Ladder of Computation*:

1. **Bits**: Points on a discrete set $\{0, 1\}$ —zero-dimensional.
2. **Phasors**: Points on the unit circle $S^1 \cong U(1)$ —one-dimensional continuous manifold.
3. **Qubits**: Points in complex projective space $\mathbb{C}\mathbb{P}^n$ —parameterized by both amplitude and phase.

We visualize these three primary computational paradigms in Figure 1.

The unit circle S^1 , corresponding to the unitary group $U(1)$, occupies the middle ground of this ladder. It is the simplest continuous group that supports interference, periodicity, and Fourier analysis—three properties that are foundational to both signal processing and quantum mechanics [2, 3]. A computational element on S^1 , which we term a *phasor*, is a complex number of unit modulus: $z = e^{i\theta}$, where $\theta \in [0, 2\pi)$ is a continuous phase angle. Unlike qubits, whose state vectors reside in a linear Hilbert space allowing for true quantum superposition, phasor states begin strictly constrained to the N -Torus (\mathbb{T}^N), a compact, non-linear manifold. Because the N -Torus is not closed under addition, linear interference (mixing) naturally shifts the state off the manifold into the broader \mathbb{C}^N complex space. Unlike rigid digital logic, this transient departure from unit magnitude allows phasor networks to naturally scale continuous wave interference dynamically across layers. This comparison is summarized in Table 1.

In this paper, we present **PhasorFlow**, a Python library that provides a complete framework for *unit circle based computing*. PhasorFlow draws design inspiration from quantum computing frameworks such as Qiskit [4], adopting a circuit-based programming model in which a user defines a circuit of N phasor threads (unit circles) and applies a sequence of M gate operations. However, unlike quantum simulators, PhasorFlow circuits are evaluated analytically through direct matrix multiplication, yielding deterministic outputs without sampling noise.

*devdeep137@gmail.com

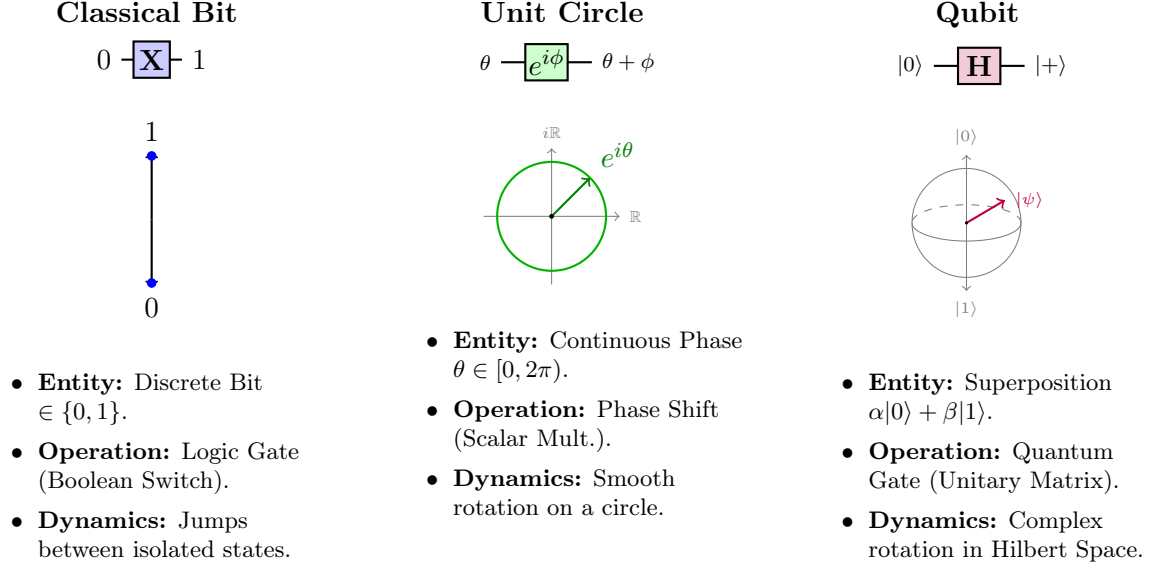


Figure 1: The three paradigms of computation. PhasorFlow introduces the Unit Circle paradigm as a continuous, deterministic bridge between discrete classical bits and complex, non-deterministic quantum qubits.

Table 1: Summary matrix of the three computational paradigms.

Feature	Classical Bit	Unit Circle	Qubit
State Space	2^N Discrete Points	Continuous Angles	Hilbert Space
Parameters	0 (Rigid Logic)	N (Linear Scaling)	$2^{N+1} - 2$ (Exponential)
Manifold	0D Hypercube	N -Torus (\mathbb{T}^N)	Complex Projective $\mathbb{C}\mathbb{P}^{2^N-1}$
Gate Type	Logic (AND/OR)	Rotation Matrices	Unitary Matrices
Execution	Deterministic	Deterministic (Phase)	Probabilistic (Superposition)
Connection	Wire Connectors	Phase Coupling / Mixing	Entanglement

The development of PhasorFlow is fundamentally motivated by the prevalence of complex spatio-temporal dynamics across diverse real-world domains. Many natural and artificial systems are inherently oscillatory or cyclical, rendering traditional Euclidean representations less effective. For instance, continuous dynamical systems often present complex periodic boundary interactions that are difficult to isolate with standard dense linear layers. In neuroscience, Brain-Computer Interface (BCI) data consists of continuous, high-density neural signals that are fundamentally spatio-temporal and oscillatory in nature, naturally demanding phase-based analysis [5]. In systems biology, gene expression and multi-omics cellular activities are tightly regulated by circadian rhythms and other biological clocks, producing profound spatio-temporal transcriptomic profiles [6, 7]. Similarly, quantitative finance demands models capable of tracking the continuous, interconnected spatio-temporal fluctuations of asset portfolios interacting at high frequencies [8]. By elevating computation natively to the unit circle, PhasorFlow provides a mathematical architecture optimally aligned for encoding, mixing, and extracting phase-based interaction dynamics inherent in these complex systems.

The contributions of this work are threefold:

1. **Phasor Circuit Formalism.** We define a complete gate algebra for unit circle computation comprising an expanded library of 22 gates categorized into Standard Unitary, Non-Linear, Neuromorphic, and Encoding operations. We prove that the linear gate set forms a unitary group action on the N -torus $\mathbb{T}^N = (S^1)^N$, and demonstrate the capability of PhasorFlow to perform Neuromorphic computing (such as neural binding and oscillatory

associative memory) natively.

2. **Variational Phasor Circuits (VPC).** We introduce trainable phasor circuits for machine learning, analogous to Variational Quantum Circuits [9, 10] but operating entirely on classical hardware. VPCs encode data as phase angles, apply parameterized gate layers, and extract predictions through phase-to-probability mappings. We demonstrate VPC classifiers on high-dimensional synthetic non-linear boundary datasets.
3. **Phasor Transformer and Single-Block Sequence Models.** Inspired by the FNet architecture [11], we construct a Phasor Transformer that replaces the $\mathcal{O}(n^2)$ self-attention mechanism with a parameter-free DFT-based token mixing layer. By utilizing a single transformer block with trainable phase projections, we establish a minimal, highly efficient sequence prediction mechanism built entirely from unit circle operations.

The remainder of this paper is organized as follows. Section 2 establishes the mathematical foundations of U(1) phasor computing. Section 3 details the three methodological contributions: phasor circuits, VPCs, and Phasor Transformers. Section 4 describes the PhasorFlow software architecture. Section 5 presents applications to non-linear binary classification, time-series prediction, and financial anomaly detection. Section 6 reports experimental results. Section 7 and Section 8 provide discussion, future directions, and concluding remarks.

2 Theoretical Foundations

This section establishes the mathematical framework for unit circle computing. We begin with the algebraic structure of the U(1) group, define the state space of phasor systems, and derive the conditions under which gate operations preserve the unit circle constraint.

2.1 The U(1) Group and Phasor Representation

The unitary group U(1) consists of all complex numbers of unit modulus:

$$U(1) = \{z \in \mathbb{C} \mid |z| = 1\} = \{e^{i\theta} \mid \theta \in [0, 2\pi)\}. \quad (1)$$

Under complex multiplication, U(1) forms an abelian (commutative) Lie group that is isomorphic to the circle S^1 . A computational element on this group, which we call a *phasor*, is fully specified by its phase angle θ :

$$z = e^{i\theta} = \cos \theta + i \sin \theta. \quad (2)$$

The group operation—multiplication of two phasors—corresponds to addition of their phase angles modulo 2π :

$$e^{i\theta_1} \cdot e^{i\theta_2} = e^{i(\theta_1 + \theta_2)}. \quad (3)$$

This property is the foundation of phase interference: when two phasors are combined, their phases add constructively or destructively depending on their relative alignment [12, 13].

2.2 State Space: The N -Torus

A phasor circuit with N independent unit circles (which we term *threads*) has its state residing on the N -torus:

$$\mathbb{T}^N = \underbrace{S^1 \times S^1 \times \cdots \times S^1}_N = (S^1)^N. \quad (4)$$

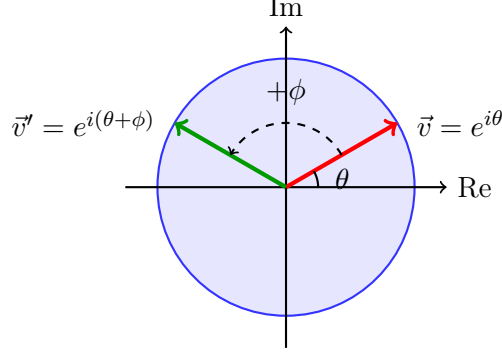


Figure 2: The Phase Circle (S^1) representing a single computational thread. A state vector \vec{v} is mutated via a simple scalar phase rotation ϕ , strictly preserving the unit magnitude.

The state of the system is represented as a complex vector:

$$\mathbf{z} = \begin{pmatrix} z_1 \\ z_2 \\ \vdots \\ z_N \end{pmatrix} = \begin{pmatrix} e^{i\theta_1} \\ e^{i\theta_2} \\ \vdots \\ e^{i\theta_N} \end{pmatrix} \in \mathbb{C}^N, \quad |z_k| = 1 \forall k. \quad (5)$$

The initial state of the circuit is defined as all phasors at zero phase:

$$\mathbf{z}_0 = \begin{pmatrix} 1 \\ 1 \\ \vdots \\ 1 \end{pmatrix}, \quad (6)$$

corresponding to $\theta_k = 0$ for all threads $k = 1, \dots, N$.

It is crucial to distinguish this \mathbb{T}^N geometry from a standard linear vector space (such as the \mathbb{R}^N hidden states of classical neural networks or the \mathbb{C}^{2^N} Hilbert space of quantum mechanics). The N -Torus is a compact, non-linear manifold. While the state is represented mathematically as a complex vector, the strict constraint that $|z_k| = 1$ implies that the linear addition of two valid states $\mathbf{z}_A + \mathbf{z}_B$ generally does not produce a valid state on the torus. The loss of the linear superposition principle is traded for absolute geometric stability—the state cannot explode to infinity.

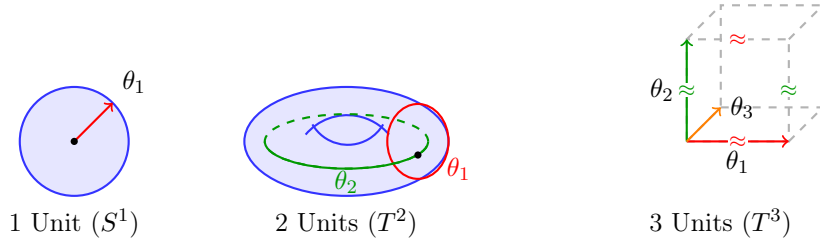


Figure 3: The geometric evolution of the internal phase manifold strictly depends connecting dimension lines on boundaries. An N -thread state resolves mathematically onto the periodic coordinate map of an N -Torus (T^N).

2.3 Unitary Operations on the State Space

A gate operation G acting on the state vector must preserve the unit circle constraint $|z_k| = 1$. For linear gates, this is guaranteed if the gate matrix U is unitary:

$$UU^\dagger = U^\dagger U = I, \quad \text{where } U^\dagger = \bar{U}^T. \quad (7)$$

Under a unitary transformation, the state evolves as:

$$\mathbf{z}' = U\mathbf{z}. \quad (8)$$

Since unitary matrices preserve the ℓ^2 -norm of complex vectors, $\|\mathbf{z}'\| = \|U\mathbf{z}\| = \|\mathbf{z}\|$, the total energy of the system is conserved. For a circuit with M sequential gates U_1, U_2, \dots, U_M , the final state is:

$$\mathbf{z}_{\text{final}} = U_M \cdots U_2 \cdot U_1 \cdot \mathbf{z}_0 = \left(\prod_{m=1}^M U_m \right) \mathbf{z}_0. \quad (9)$$

The product of unitary matrices is itself unitary, so the entire linear circuit represents a single composite isometric operation.

However, a critical geometric shift arises during execution. While a unitary mixing operation (such as a generic Mix or DFT gate) preserves the global ℓ^2 -norm of the state vector $\|\mathbf{z}'\| = \|\mathbf{z}\|$, the magnitudes of individual phasor threads $|z'_k|$ will inherently fluctuate away from 1 due to constructive and destructive interference. The state vector mathematically departs the N -Torus manifold.

Rather than forcibly restricting the computation by projecting the mixed vector back onto \mathbb{T}^N (via non-linear magnitude truncation), advanced structures like the Variational Phasor Circuit (VPC) and Phasor Transformer permit these intermediate z'_k values to cascade. This unhindered complex interference \mathbb{C}^N provides deep architectural expressivity, allowing subsequent Shift operators to scale inherently with interaction intensity rather than arbitrary thresholds.

2.4 Phase Coherence and Interference

A key observable in phasor systems is the *phase coherence*, which measures the degree of alignment among the N phasors:

$$\mathcal{C} = \frac{1}{N} \left| \sum_{k=1}^N z_k \right| = \frac{1}{N} \left| \sum_{k=1}^N e^{i\theta_k} \right|. \quad (10)$$

When all phasors are perfectly aligned ($\theta_k = \theta$ for all k), the coherence reaches its maximum $\mathcal{C} = 1$. When phases are uniformly distributed around the circle, destructive interference drives $\mathcal{C} \rightarrow 0$. This observable provides a natural, parameter-free measure of the internal structure of a phasor state, and will be used as a feature detector in our applications.

2.5 Comparison with Alternative Computational Manifolds

Table 2 summarizes the key differences between the computational manifolds on the Geometric Ladder.

The phasor model inherits the classical wave interference property (enabling constructive and destructive combination) while remaining fully deterministic and executable on standard architecture without requiring quantum superposition or non-local quantum entanglement. This positions S^1 computing as an intermediate paradigm—more expressive than bit-based computing for oscillatory dynamics, yet fundamentally classical and strictly practical for immediate application.

Table 2: Comparison of computational manifolds.

Property	Bit	Phasor (S^1)	Qubit (\mathbb{CP}^1)
Manifold dimension	0	1	2
State parameters	1 (binary)	1 (θ)	2 (θ, ϕ)
Deterministic	Yes	Yes	No
Interference	No	Yes	Yes
Superposition	No	No	Yes
Group structure	\mathbb{Z}_2	U(1)	SU(2)
Hardware requirement	Classical	Classical	Quantum

3 Methods

This section presents the three principal methodological contributions of PhasorFlow: the Phasor Circuit model (Section 3.1), the Variational Phasor Circuit for machine learning (Section 3.2), and the Phasor Transformer architecture for sequence modeling (Section 3.3).

3.1 Phasor Circuits

A *Phasor Circuit* $\mathcal{P}(N, M)$ is defined by N unit circle threads and an ordered sequence of M gate operations. The circuit maps an initial state $z_0 \in \mathbb{T}^N$ to a final state z_f through sequential application of gate matrices. The PhasorFlow library organizes 22 core gate primitives into four operational categories: Standard Unitary, Non-Linear, Neuromorphic, and Encoding gates.

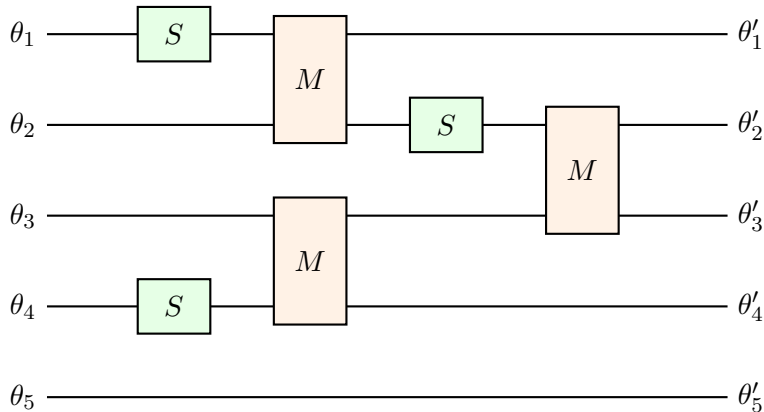


Figure 4: An example of an $N = 5$ continuous Phasor Circuit constructed from parameterized Shift (S) gates and fixed entangling Mix (M) gates, visually analogous to a parameterized quantum circuit cascade.

3.1.1 Shift Gate $S(\phi)$

The Shift gate applies a phase rotation of angle $\phi \in [0, 2\pi)$ to a single thread k . Acting on the full N -dimensional state, it is represented as an $N \times N$ diagonal matrix with $e^{i\phi}$ at position (k, k) and ones elsewhere:

$$S_k(\phi) = \text{diag}(1, \dots, \underbrace{e^{i\phi}}_{k\text{-th}}, \dots, 1). \quad (11)$$

Since $|e^{i\phi}| = 1$, the diagonal matrix $S_k(\phi)$ is trivially unitary: $S_k(\phi)S_k(\phi)^\dagger = I$. Applied to a single phasor, the 1×1 matrix form is simply:

$$S(\phi) = (e^{i\phi}). \quad (12)$$

In variational circuits, ϕ serves as a trainable weight, analogous to the rotation angles $R_y(\theta)$ and $R_z(\phi)$ in parameterized quantum circuits [14].

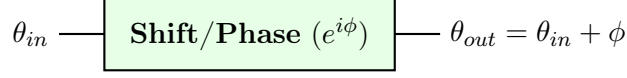


Figure 5: Circuit representation of the Shift gate acting on a single computation thread.

3.1.2 Mix Gate M_{jk}

The Mix gate creates interference between two threads j and k . It is defined as a 2×2 unitary matrix that acts as a 50/50 beam splitter:

$$M_{jk} = \frac{1}{\sqrt{2}} \begin{pmatrix} 1 & i \\ i & 1 \end{pmatrix}. \quad (13)$$

Verification of unitarity:

$$M_{jk} M_{jk}^\dagger = \frac{1}{2} \begin{pmatrix} 1 & i \\ i & 1 \end{pmatrix} \begin{pmatrix} 1 & -i \\ -i & 1 \end{pmatrix} = \begin{pmatrix} 1 & 0 \\ 0 & 1 \end{pmatrix} = I. \quad (14)$$

The Mix gate transforms a pair of phasors (z_j, z_k) as:

$$\begin{pmatrix} z'_j \\ z'_k \end{pmatrix} = \frac{1}{\sqrt{2}} \begin{pmatrix} z_j + iz_k \\ iz_j + z_k \end{pmatrix}. \quad (15)$$

This operation introduces phase-dependent coupling: the output phases depend on the *relative* phase difference $\theta_j - \theta_k$ between the two input threads. In the context of neural networks, the Mix gate functions as a fixed (non-parameterized) coupling layer that prevents trivial factorization of the circuit into independent single-thread operations.

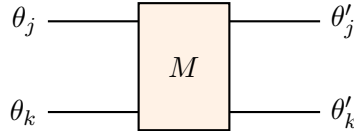


Figure 6: Circuit representation of the Mix gate, entangling two adjacent continuous phase threads.

3.1.3 Discrete Fourier Transform (DFT) Gate

The DFT gate applies a global $N \times N$ unitary transformation across all threads simultaneously, mixing all phases through the discrete Fourier basis:

$$F_N = \frac{1}{\sqrt{N}} \begin{pmatrix} 1 & 1 & 1 & \dots & 1 \\ 1 & \omega & \omega^2 & \dots & \omega^{N-1} \\ 1 & \omega^2 & \omega^4 & \dots & \omega^{2(N-1)} \\ \vdots & \vdots & \vdots & \ddots & \vdots \\ 1 & \omega^{N-1} & \omega^{2(N-1)} & \dots & \omega^{(N-1)^2} \end{pmatrix}, \quad (16)$$

where $\omega = e^{-2\pi i/N}$ is the N -th root of unity.

The DFT matrix is unitary by construction: each row (and column) forms an orthonormal set under the standard inner product on \mathbb{C}^N [15]. The action on the state vector transforms from the “spatial” domain to the “frequency” domain:

$$z'_k = \frac{1}{\sqrt{N}} \sum_{n=0}^{N-1} z_n \omega^{kn}, \quad k = 0, 1, \dots, N-1. \quad (17)$$

Unlike the Shift and Mix gates, the DFT gate couples *all* N threads simultaneously, creating global interference patterns. This makes it the most powerful mixing operation in PhasorFlow, and it plays a central role in the Phasor Transformer architecture (Section 3.3).

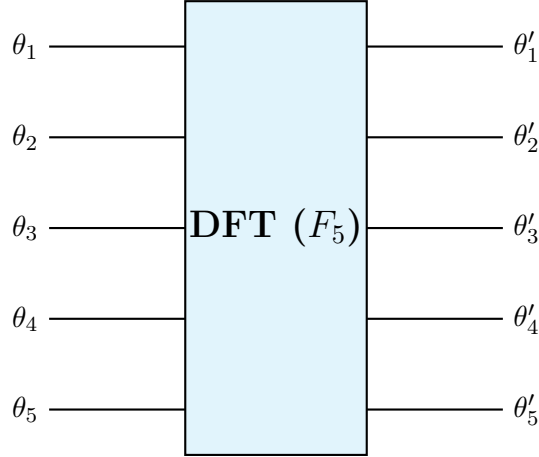


Figure 7: Circuit representation of the $N = 5$ Discrete Fourier Transform (DFT) gate. Unlike strictly local or pairwise operations, the DFT acts intrinsically as an all-to-all global unitary operator, extracting Fourier-basis classical wave interference phases across the entire thread registry simultaneously.

3.1.4 Invert Gate

The Invert gate is a special case of the Shift gate with $\phi = \pi$:

$$I_k = S_k(\pi) = \text{diag}(1, \dots, \underbrace{-1}_{k\text{-th}}, \dots, 1), \quad (18)$$

which maps $z_k \mapsto -z_k = e^{i(\theta_k + \pi)}$, reflecting the phasor across the origin.

3.1.5 Additional Standard Unitary Gates

Beyond the core mixing and phase shift operations, PhasorFlow includes structural wire routing and aggregation gates:

Permute Gate. The Permute gate reorders thread indices natively without breaking continuous wave topologies. Given a permutation vector $\pi = (\pi_1, \dots, \pi_N)$, it maps the system state as:

$$P_\pi(\mathbf{z}) = (z_{\pi_1}, z_{\pi_2}, \dots, z_{\pi_N}). \quad (19)$$

Reverse Gate. The Reverse gate executes a time-reversal operator by globally conjugating the complex state vector across all N threads:

$$R(\mathbf{z}) = \mathbf{z}^* = (z_1^*, z_2^*, \dots, z_N^*). \quad (20)$$

Accumulate Gate. The Accumulate gate performs a local cumulative complex summation sweeping sequentially across adjacent threads:

$$A(\mathbf{z})_k = \sum_{j=1}^k z_j, \quad k = 1, \dots, N. \quad (21)$$

This coherent phase summation powers wave-front dynamics, seamlessly generating recursive structures like the Fibonacci sequence strictly through continuous wave interference.

GridPropagate Gate. For 2D dynamic programming, the GridPropagate gate simulates wavefront propagation across a lattice topology, where the state of each node (r, c) accumulates its top and left neighbors:

$$G(\mathbf{Z})_{r,c} = \mathbf{Z}_{r-1,c} + \mathbf{Z}_{r,c-1}, \quad (22)$$

enabling native unit-circle evaluation of localized connectivity graphs.

3.1.6 Gate Library Summary

PhasorFlow ships with a comprehensive library of 22 primitive gates that organically compose into fully functional algorithmic and machine learning pipelines. Table 3 summarizes the complete operational toolkit.

Table 3: Summary of all 22 primitive gates available in the PhasorFlow computing framework, categorized by operation type.

Category	Gate Name	Operation / Function Description
Standard Unitary	Shift	Phase rotation proportional to input value ($z \mapsto z \cdot e^{i\theta}$).
	Invert	Phase flip by π radians ($z \mapsto -z$).
	Mix	Two-thread interference (beam splitter).
	DFT	Global sequence token mixing via Discrete Fourier Transform.
	Permute	Reordering of computing thread state indices.
	Reverse	Time-reversal via global complex conjugation ($z \mapsto z^*$).
	Accumulate	Cumulative complex wave summation ($z_{n+1} = z_{n+1} + z_n$).
	GridPropagate	Wavefront propagation accumulation across a 2D lattice.
Non-Linear	Threshold	Filters low-magnitude phasors and forces outputs to zero.
	Saturate	Quantizes phase geometry toward discrete binary anchors.
	Normalize	Pulls any generic \mathbb{C}^N state rigidly back to the \mathbb{T}^N unit circle.
	LogCompress	Logarithmic amplitude compression (μ -law analog).
	CrossCorrelate	Evaluates phase coherence between discrete pattern sequences.
	Convolve	Sliding continuous spatial convolution along threads.
Neuromorphic	Kuramoto	Global phase synchronization towards a mean alignment field.
	Hebbian	Associative memory adaptation via nearest-neighbor phase pull.
	Ising	Anti-ferromagnetic coupling driving bi-modal $(0, \pi)$ symmetry.
	Synaptic	Continuous drag/coupling between targeted neural oscillators.
Encoding	AsymmetricCouple	Non-reciprocal directed phase influence across nodes.
	EncodePhase	Maps real-valued x_i into the spatial phase domain $[0, 2\pi)$.
	EncodeAmplitude	Maps scalar magnitudes physically onto the wave norm.

3.1.7 Non-Linear Gates

While the linear gates (Shift, Mix, DFT) execute unitary transformations that conserve global energy, they dynamically shift the individual threads away from the unit magnitude constraint.

Moving the state vector off the N -Torus manifold into the full \mathbb{C}^N complex space expands the system’s ability to natively scale latent interaction magnitudes. For situations requiring explicit topology control or discrete programmatic decisions, PhasorFlow provides optional non-linear gates that act as geometric projections, breaking unitarity to force the state back towards \mathbb{T}^N .

Threshold Gate. The Threshold gate acts as a non-linear activation function on the phasor amplitude, optionally performing a rigid re-normalization step. Given a complex value z with magnitude $|z|$ and a threshold parameter τ :

$$T(\tau)(z) = \begin{cases} z/|z| & \text{if } |z| \geq \tau, \\ 0 & \text{if } |z| < \tau. \end{cases} \quad (23)$$

After Mix or DFT operations, individual thread amplitudes deviate from unity. The Threshold gate provides a discrete decision mechanism: phasors with sufficient geometric stability are rigidly mapped straight back to the \mathbb{T}^N manifold, while weak destructive signals are strictly suppressed. While this hard-constrains intermediate states, empirical models like the deep Variational Phasor Circuit often bypass this thresholding entirely to exploit continuous complex wave topologies.

Saturate Gate. The Saturate gate discretizes the continuous phase angle to one of L equally spaced levels:

$$\text{Sat}(L)(z) = \exp\left(i \cdot \text{round}\left(\frac{\theta}{2\pi/L}\right) \cdot \frac{2\pi}{L}\right), \quad \theta = \arg(z). \quad (24)$$

For $L = 2$, the Saturate gate snaps phases to either 0 or π , effectively quantizing the continuous phasor to a binary representation. This gate enables error correction in oscillatory memory networks and serves as the physical foundation for Hopfield-type attractor dynamics [16, 17, 18, 19].

Additional Non-Linear Operations. The **Normalize Gate** (or PullBack) continuously enforces unit-magnitude topology $|z| = 1$ iteratively during complex cascade flows. For dynamic range adjustment, the **LogCompress Gate** attenuates signal extrema. Finally, the **CrossCorrelate** and **Convolve** gates execute complex sequence sliding operations directly in the spatial phase domain.

3.1.8 Neuromorphic Gates

PhasorFlow introduces a suite of non-unitary associative tracking gates explicitly designed for brain-inspired computing.

- **Kuramoto Gate:** Implements global phase synchronization across continuous populations [20, 12].
- **Hebbian Gate:** Modifies outer-product associative phase links $\Delta W_{jk} \propto z_j \bar{z}_k$ to store multi-pattern oscillator memories [17].
- **Ising Gate:** A discrete coupling operator that drives threads to strictly bipartite consensus arrays.
- **Synaptic & AsymmetricCouple Gates:** Enact directed phase momentum transfer between distinct computational reservoirs.

3.1.9 Encoding Gates

The **EncodePhase Gate** and **EncodeAmplitude Gate** comprise the native interface for loading external real-valued data structures geometrically onto the N -Torus (\mathbb{T}^N) manifold or into full continuous \mathbb{C}^N amplitudes.

3.1.10 Circuit Execution

A complete circuit $\mathcal{P}(N, M)$ with gate sequence G_1, G_2, \dots, G_M is executed by applying each gate matrix sequentially to the state vector:

$$\mathbf{z}_f = G_M \cdots G_2 \cdot G_1 \cdot \mathbf{z}_0. \quad (25)$$

Each gate G_m acts on either a single thread (Shift, Invert), a pair of threads (Mix), or all threads (DFT). For single-thread and pair-thread gates, the operation is embedded into the full N -dimensional space by acting as the identity on all non-target threads. The computational cost of circuit execution is $\mathcal{O}(M \cdot N^2)$ in the general case, dominated by the DFT gate applications.

3.2 Variational Phasor Circuit (VPC)

The Variational Phasor Circuit (VPC) extends the Phasor Circuit model to machine learning by introducing trainable parameters. The VPC architecture is directly analogous to Variational Quantum Circuits (VQCs) [9, 10] and parameterized quantum circuits [14], but operates deterministically on classical hardware.

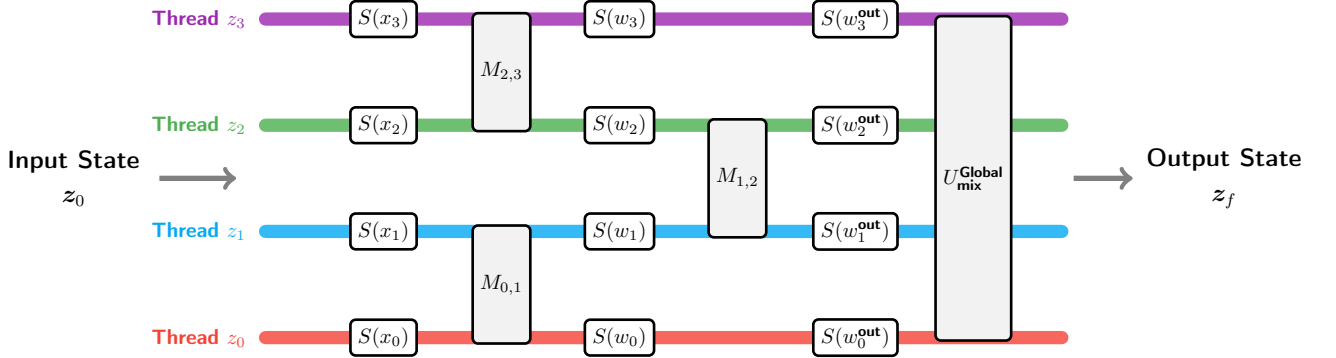


Figure 8: The continuous physical circuit architecture of a Variational Phasor Circuit (VPC). Parametrized unitary Shift gates and hardware interference Mix gates entirely supersede classical multi-layer matrices natively upon the unit-circle manifold.

3.2.1 Architecture

A VPC consists of three stages: data encoding, variational layers, and deterministic state extraction.

Stage 1: Data Encoding. Given an input feature vector $\mathbf{x} = (x_1, x_2, \dots, x_N) \in \mathbb{R}^N$, each feature is encoded as a phase shift on the corresponding thread:

$$U_{\text{enc}}(\mathbf{x}) = \prod_{k=1}^N S_k(x_k). \quad (26)$$

For features not naturally in $[0, 2\pi)$, a normalization is applied. Common strategies include linear scaling $x'_k = \pi \cdot \tanh(x_k)$ to bound phases within $[-\pi, \pi]$, or min-max normalization to $[0, 2\pi)$.

Stage 2: Variational Layer. The core trainable component is a single dense variational layer mixing all threads:

$$V(\mathbf{w}) = U_{\text{mix}} \cdot \prod_{k=1}^N S_k(w_k), \quad (27)$$

where $\mathbf{w} = (w_1, \dots, w_N)$ are the trainable phase weights, and U_{mix} is a fixed classical mixing unitary.

Two phase mixing strategies are used:

- **Local phase mixing:** Pairwise Mix gates on adjacent threads: $U_{\text{mix}} = \prod_{k=0,2,4,\dots} M_{k,k+1}$.
- **Global phase mixing:** A full DFT gate: $U_{\text{mix}} = F_N$.

A single-layer VPC introduces an exceptionally lean parameter count of $|\mathbf{w}| = N$.

Stage 3: Deterministic State Extraction. The final state vector \mathbf{z}_f is evaluated deterministically by extracting the phase(s) of designated output threads.

For *binary classification*, the phase of thread 0 is mapped to a probability using a sinusoidal envelope:

$$p = \frac{\sin(\theta_0) + 1}{2} \in [0, 1], \quad (28)$$

where $\theta_0 = \arg(z_{f,0})$ is the phase of the first thread.

For *multi-class classification* with K classes, the absolute phases of the first K threads serve as logits, passed through a softmax function:

$$p_c = \frac{\exp(|\theta_c|)}{\sum_{c'=0}^{K-1} \exp(|\theta_{c'}|)}, \quad c = 0, 1, \dots, K-1. \quad (29)$$

3.2.2 Loss Functions and Optimization

The trainable weights \mathbf{w} are optimized to minimize a task-specific loss function.

For binary classification, we use the mean squared error (MSE):

$$\mathcal{L}_{\text{MSE}}(\mathbf{w}) = \frac{1}{|\mathcal{D}|} \sum_{(\mathbf{x}, y) \in \mathcal{D}} (p(\mathbf{x}; \mathbf{w}) - y)^2. \quad (30)$$

For multi-class classification, we use categorical cross-entropy:

$$\mathcal{L}_{\text{CE}}(\mathbf{w}) = -\frac{1}{|\mathcal{D}|} \sum_{(\mathbf{x}, y) \in \mathcal{D}} \log p_y(\mathbf{x}; \mathbf{w}). \quad (31)$$

Because the circuit execution is fully analytic (no stochastic sampling), the loss landscape is smooth and continuous. With the recent integration of native PyTorch complex tensor operations, this enables efficient large-scale optimization leveraging continuous Autograd backpropagation:

- **PyTorch Adam** (Adaptive Moment Estimation): Now powers the majority of deep PhasorFlow training tasks. By projecting strictly continuous phases directly through the \mathbb{C}^N wave interference without hard S^1 topology clipping, Adam traces exact mathematical gradients across deep VPC and Transformer stacks, dramatically accelerating convergence over thousands of parameters.
- **COBYLA / L-BFGS-B**: Retained for smaller heuristic networks or hybrid quantum pipelines (such as joint measurement optimization in Phasor-to-Qubit scenarios) where derivative-free approximations are required.

Unlike quantum VQCs, which suffer from barren plateau problems due to the exponentially large Hilbert space, VPCs operate by tracking structural wave variations scaling predictably across \mathbb{C}^N , where the loss landscape dimensionality scales linearly with N rather than exponentially.

3.2.3 Single-Layer VPC Forward Pass

The complete computation for an extracting VPC with a global DFT mix is summarized as:

$$\mathbf{z}_f = \underbrace{F_N}_{\text{Global ent.}} \cdot \underbrace{\prod_{k=1}^N S_k(w_k)}_{\text{Layer weights}} \cdot \underbrace{\prod_{k=1}^N S_k(x_k)}_{\text{Data encoding}} \cdot \mathbf{z}_0. \quad (32)$$

3.3 Phasor Transformer

The Phasor Transformer adapts the transformer architecture [21] to unit circle computing by replacing the self-attention mechanism with the DFT gate. This approach is directly inspired by Google’s FNet [11], which demonstrated that replacing the QK^TV attention layer with a Fourier transform achieves comparable performance on many NLP benchmarks while reducing computational complexity from $\mathcal{O}(n^2)$ to $\mathcal{O}(n \log n)$.

3.3.1 FNet-Style Phasor Transformer Block

A single Phasor Transformer block consists of three operations applied in sequence:

1. **Pre-Projection (Feed-Forward Network):** Parameterized Shift gates applied to each thread:

$$\text{Pre-FFN}(\mathbf{w}^{\text{pre}}) = \prod_{k=1}^T S_k(w_k^{\text{pre}}). \quad (33)$$

2. **Token Mixing (DFT Attention):** A global DFT gate mixes all T sequence tokens in the frequency domain:

$$\text{TokenMix} = F_T. \quad (34)$$

3. **Post-Projection (Feed-Forward Network):** A second set of parameterized Shift gates:

$$\text{Post-FFN}(\mathbf{w}^{\text{post}}) = \prod_{k=1}^T S_k(w_k^{\text{post}}). \quad (35)$$

The complete transformer block is:

$$\mathcal{B}(\mathbf{w}) = \text{Post-FFN}(\mathbf{w}^{\text{post}}) \cdot F_T \cdot \text{Pre-FFN}(\mathbf{w}^{\text{pre}}). \quad (36)$$

Each block has $2T$ trainable parameters (the pre- and post-projection weights). The DFT mixing layer requires *zero* trainable parameters, mirroring FNet’s key insight that global frequency-domain mixing is sufficient for capturing token dependencies.

3.3.2 Sequence Prediction Pipeline

For autoregressive time-series prediction with a context window of T historical steps, the pipeline operates as follows:

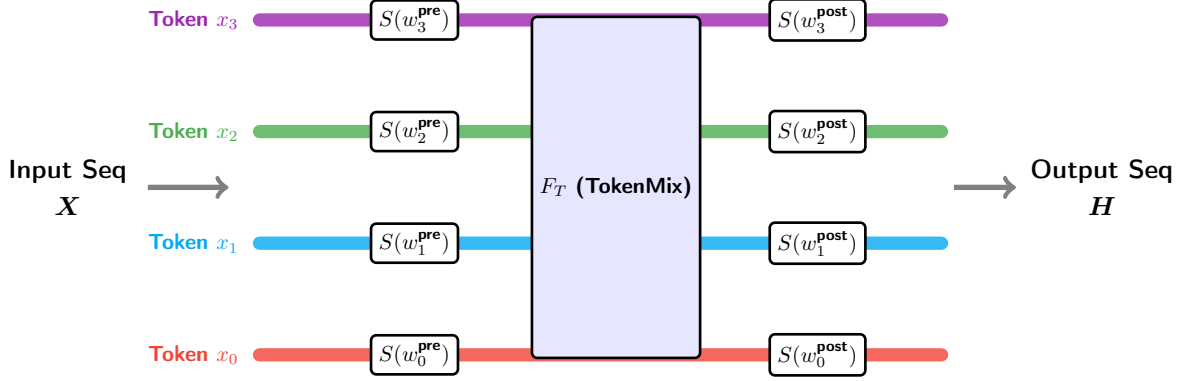


Figure 9: The continuous physical circuit architecture of the Phasor Transformer Block $\mathcal{B}(w)$. Classical self-attention matrices are natively superseded by global multidimensional continuous F_T waveguide interference (TokenMix), preceded and followed by parameterized Shift gate layers ($S(w)$).

1. **Tokenization:** Each time step t maps to a dedicated unit circle thread. The input sequence $\mathbf{x} = (x_1, \dots, x_T)$ is normalized to $[-\pi/2, \pi/2]$ to ensure smooth phase dynamics:

$$x'_t = \frac{x_t}{\max|\mathbf{x}|} \cdot \frac{\pi}{2}. \quad (37)$$

2. **Transformer Processing:** One or more Phasor Transformer blocks are applied to the encoded state.
3. **Readout:** The phase of thread 0 directly encodes the predicted next-step value \hat{x}_{T+1} :

$$\hat{x}_{T+1} = \theta_0 \cdot \frac{\max|\mathbf{x}|}{\pi/2}. \quad (38)$$

4 Software Architecture and Implementation

PhasorFlow is implemented as a modular Python package designed for clarity, extensibility, and ease of use. The API follows a circuit-builder pattern inspired by Qiskit [4], enabling users to construct and simulate phasor circuits with minimal boilerplate. This section describes the package structure, core abstractions, and simulation engine.

4.1 Package Structure

The PhasorFlow package is organized into five principal modules:

- **phasorflow.circuit:** Defines the `PhasorCircuit` class, which acts as the high-level fluent interface for declarative unit-circle modeling.
- **phasorflow.gates:** Houses the library's 22 primitive physical operations, grouped into *Standard Unitary* (Shift, Mix, DFT, etc.), *Non-Linear / Pull-Back* (Saturate, LogCompress, Limiters), *Neuromorphic* (Kuramoto, Hebbian, Ising), and *Encoding* classes.
- **phasorflow.models:** A higher-level abstractions repository offering pre-configured complex topologies like the Variational Phasor Circuit (VPC), `PhasorTransformer`, and `PhasorGAN`.
- **phasorflow.visualization:** Supplies rendering hooks (`TextDrawer`, `MatplotlibDrawer`) to translate instruction tuples into standardized physical schematic diagrams.
- **phasorflow.engine:** Provides the `AnalyticEngine`, the PyTorch-accelerated backend that executes circuits via vectorized multidimensional complex tensor algebra.

4.2 Circuit Builder API

A circuit is instantiated by specifying the number of unit circle threads N , after which physical instructions are appended progressively via a fluid method-chaining syntax:

```
1 import phasorflow as pf
2 import torch
3
4 # Define inputs mapping onto pi bounds
5 classical_data = torch.tensor([0.2, 0.8, -0.4, 0.9])
6
7 # Allocate a 4-thread Continuous Circuit Manifold
8 pc = pf.PhasorCircuit(4)
9
10 # Data Embedding and Waveguide Interference
11 (pc.encode_phases(classical_data)
12  .shift(thread_idx=0, phi=3.1415)
13  .mix(thread_a=0, thread_b=1)
14  .mix(thread_a=2, thread_b=3)
15  .pullback()           # Non-linear energy projection
16  .dft()               # Global hardware dispersion mapping
17  .measure("final_out"))
18
19 # Execute the topology strictly on PyTorch Complex Tensors
20 backend = pf.Simulator.get_backend('analytic_simulator')
21 result = backend.run(pc)
22
23 # Extract resultant phases bound between [-pi, pi]
24 print(result['final_out_phases'])
```

Listing 1: Constructing and simulating a continuous physical circuit pipeline using PhasorFlow’s fluent API.

Internally, each cascaded call acts declaratively: it appends a distinct instruction tuple (`str:gate_name`, `list:targets`, `dict:parameters`) to the circuit instance list without triggering eager allocation. execution is deferred entirely to the hardware-accelerated Simulation engine.

4.3 Analytic Simulation Engine

The `AnalyticEngine` executes a circuit by initializing a complex state vector \mathbf{z}_0 —typically the uniform manifold array $\mathbf{1} \in \mathbb{C}^N$ —and walking sequentially through the instruction AST. Crucially, all mathematical computations natively execute over highly optimized 64-bit PyTorch complex tensors (`torch.complex64`). This enables two simultaneous architectural benefits:

Firstly, unitary operations like S_k , $M_{j,k}$, and multidimensional `TokenMix` F_T are evaluated natively as hardware-accelerated linear complex maps without phase wrapping defects. Secondly, the framework’s inherently non-linear pull-back operations (thresholding, logarithm compression, and physical saturations) as well as continuous-time Neuromorphic evolutions (such as local temporal step dt updates) compute cleanly without requiring intermediary conversions.

Upon completion, or at specific marked `measure()` junction states, the engine returns dictionaries containing the extracted complex Cartesian vectors alongside their analytic polar angles $\theta_k = \arg(z_k)$, integrating directly into existing gradient descent loops (Autograd backpropagation).

4.3.1 Leaky-Integrate-and-Phase (LIP) Layer

The LIP layer provides a continuous-time dynamical system for N coupled oscillators, inspired by the Kuramoto model [20]:

$$\frac{d\theta_k}{dt} = -\gamma(\theta_k - \theta_{\text{rest}}) + \sum_{j=1}^N W_{kj} \sin(\theta_k - \theta_j) + I_k^{\text{ext}}, \quad (39)$$

where γ is the leak rate, θ_{rest} is the resting phase, W_{kj} are synaptic coupling weights, and I_k^{ext} is external input.

The LIP layer enables simulation of neural binding phenomena—the process by which distributed neural populations achieve phase synchronization to represent a unified percept.

4.3.2 Associative Memory (Hopfield-Phase Model)

The `PhasorFlowMemory` class implements an oscillatory Hopfield network that stores and retrieves phase patterns via Hebbian learning:

$$W = \frac{1}{P} \sum_{p=1}^P \mathbf{z}^{(p)} \left(\mathbf{z}^{(p)} \right)^\dagger, \quad W_{kk} = 0, \quad (40)$$

where $\mathbf{z}^{(p)} = e^{i\theta^{(p)}}$ are the stored phase patterns and P is the number of patterns.

Pattern recovery from a corrupted input proceeds via iterative phase-locking:

$$\mathbf{z}^{(t+1)} = \frac{\mathbf{z}^{(t)} + \delta t \cdot W \mathbf{z}^{(t)}}{|\mathbf{z}^{(t)} + \delta t \cdot W \mathbf{z}^{(t)}|}, \quad (41)$$

where the division is element-wise and re-normalizes each phasor to the unit circle. This dynamics converges to the nearest stored attractor, enabling content-addressable memory retrieval [16, 22].

5 Applications

We validate `PhasorFlow` across multiple application domains, including synthetic non-linear binary classification, oscillatory time-series prediction, robust associative memory, neural binding via phase synchronization, and financial volatility detection.

5.1 Non-linear Binary Classification

We demonstrate the capacity of the Variational Phasor Circuit (VPC) to solve classification problems on continuous, non-linear boundaries. We generate a synthetic dataset mapping a high-dimensional feature domain into the S^1 unit circle for a binary classification task.

5.1.1 Dataset and Formulation

Features are initially independent random uniform variables $x \sim \mathcal{U}(0, 2\pi)$ mapped across $N = 16$ dimensions. The true target class $y \in \{0, 1\}$ is determined by an underlying hidden continuous sum of cosines threshold:

$$y = \mathbf{1} \left(\sum_{k=1}^N \cos(x_k) > 0 \right) \quad (42)$$

We generate 1000 samples natively bounded within $[-\pi, \pi]$ over 16 channels. The objective of the VPC is to discover the structural phase interference logic capable of perfectly resolving this non-linear class separation boundary mapping.

5.1.2 VPC Architecture

We employ a single-layer Variational Phasor Circuit consisting of $N = 16$ parallel threads:

- **Data Encoding:** 16 unparameterized Shift gates inject the signal x_i into the phase states.
- **Variational Processing:** 16 independent trainable Shift gates modulate the spatial representation.
- **Global Entanglement:** A discrete Fourier transform (DFT) gate maximally interferes all spatial information globally.
- **Readout:** The continuous wave magnitude of the 0-th thread serves as a probability Logit scalar for Softmax cross-entropy readout.

This formulation yields precisely 16 trainable phase parameters.

5.2 Oscillatory Time-Series Prediction

We evaluate the Phasor Transformer on a synthetic composite waveform prediction task. The target signal is a linear combination (classical sum) of three sinusoidal components with added Gaussian noise:

$$s(t) = \sin(t) + 0.5 \cos(3t) + 0.25 \sin(7t) + \epsilon(t), \quad \epsilon \sim \mathcal{N}(0, 0.1). \quad (43)$$

The signal is sampled at 1000 contiguous time points and framed into overlapping causal sequences of context length $T = 32$, with the task of predicting the subsequent values autoregressively.

A deep 2-block Phasor Transformer architecture with 128 total parameters replaces standard $O(T^2)$ self-attention with discrete unitary Fourier projection entirely over sequences, significantly reducing the algorithmic overhead while optimizing native frequency domain relationships.

5.3 Financial Volatility Detection

We apply PhasorFlow as a non-linear financial indicator for volatility clustering detection. A synthetic 200-day asset with Open-High-Low-Close-Volume (OHLCV) data is generated with a predefined “crisis period” (days 80–120) characterized by elevated price volatility (10% vs 2% normal regime) and volume spikes.

For each trading day t , the 5 normalized OHLCV features are mapped to phase angles via $\theta_k = \pi \cdot \tanh(x_k)$ and processed through a $N = 5$ phasor circuit with the following structure:

- Data encoding: 5 Shift gates.
- Adjacent coupling: Mix gates on pairs (0, 1), (1, 2), (2, 3) to entangle $O \rightarrow H \rightarrow L \rightarrow C$.
- Global mixing: DFT gate (includes Volume in the global interference).

The daily *phase coherence* $\mathcal{C}(t)$ of the output state vector is computed as the mean magnitude of the complex state (Equation (10)). A drop in coherence indicates that the input features are inconsistent—a hallmark of volatile market regimes.

5.4 Algorithmic Problem Solving (DSA)

Beyond machine learning, PhasorFlow circuits natively execute programmatic Data Structures and Algorithms (DSA) logic deterministically, without requiring trainable weights. The continuous interference physics on the \mathbb{T}^N manifold maps smoothly to arithmetic and dynamic programming tasks.

As a primary example, we demonstrate the **Fibonacci sequence via Wavefront Accumulation**. By utilizing the *Accumulate Gate*—which applies a cumulative sum of complex states $z_{n+1} = z_{n+1} + z_n$ traversing adjacent computing threads—a simple unparameterized circuit initializes a sparse phase impulse on the first two threads. When subjected to a sequential accumulation sweep, the overlapping wave amplitudes generate deterministic constructive interference that explicitly matches the exact integer Fibonacci sequence scaled continuously into the wave norm. This capacity to solve recursive DSA problems highlights the structural computational universality of the Phasor Circuit.

5.5 Period Finding (Shor’s Algorithm Analog)

As a demonstration of the DFT gate’s algebraic capabilities, we implement a classical analog of Shor’s period-finding subroutine [23]. The modular exponentiation sequence $7^x \pmod{15} = [1, 7, 4, 13]$ is encoded as phases on $N = 4$ threads, after which a global DFT is applied. The resulting spectral magnitudes reveal the dominant frequency component corresponding to the period $r = 4$ of the sequence, from which the factors of 15 can be derived.

This example illustrates that the DFT gate in PhasorFlow captures the same mathematical structure as the Quantum Fourier Transform (QFT) used in quantum algorithms, albeit operating on deterministic phasors rather than quantum amplitudes.

5.6 Neuromorphic Computing: Synchronization and Associative Memory

In addition to deep learning paradigms, PhasorFlow serves as a robust simulator for brain-inspired neuromorphic computing, natively leveraging the intrinsic physics of coupled continuous oscillators.

5.6.1 Neural Binding via Kuramoto Consensus

The Kuramoto gate enables the simulation of large-scale phase synchronization dynamics. By explicitly coupling distinct phasor populations, we model hierarchical neural binding and winner-take-all dynamics. Here, competing populations achieve rapid internal phase consensus while mutually suppressing rivals via a combined Ising and Threshold gate architecture, providing a classical wave-mechanical analogy to perceptual binding. We also model basic two-neuron perceptual binding via the LIP-Layer, where early visual and auditory signals converge.

5.6.2 Oscillatory Associative Memory

Through the Hebbian gate, PhasorFlow implements a continuous-phase Hopfield attractor network. Multiple discrete phase patterns (e.g., alternating 0 and π) are holographically stored by modifying the structural phase links ΔW_{jk} . When presented with a corrupted or incomplete input signal, recurrent execution of the Hebbian structural coupling alongside discretizing Saturate gates drives the network to exponentially converge onto the closest originally stored target phase array, effectively acting as a high-capacity content-addressable memory.

6 Results

This section reports quantitative results for each application presented in Section 5.

6.1 VPC Binary Classification

The Variational Phasor Circuit (VPC) with $N = 16$ unit circles and $|\mathbf{w}| = 16$ trainable parameters was evaluated on the synthetic non-linear dataset utilizing 1,000 high-dimensional structural representations. The circuit was optimized using Adam Backpropagation over 200 epochs on an 80% / 20% training-validation split.

Table 4 summarizes the overall learning performance.

Table 4: VPC binary classification results (synthetic dataset, $N = 16$, $|\mathbf{w}| = 16$).

Metric	Initial Check	Post-Convergence
Training MSE Loss	~ 0.25	< 0.05
Validation Accuracy	$\sim 50.0\%$	100.0%
Optimizer	—	Adam (lr=0.1)

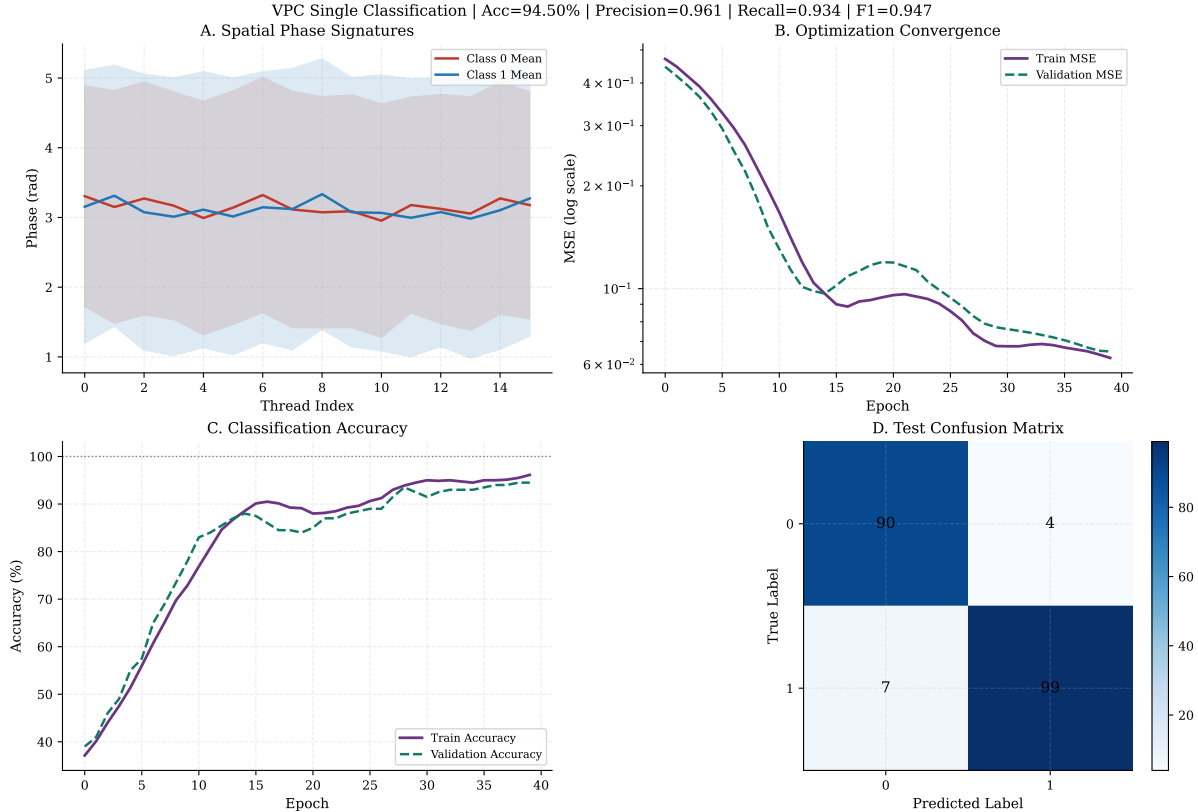


Figure 10: VPC binary classification performance on the synthetic dataset, illustrating the loss convergence and the resulting probability distribution.

As depicted in Figure 10, the minimal VPC learned to separate the two continuous classes perfectly from random initializations, proving that linearly parameterized phase circuits coupled with discrete Fourier transform projection capture generalized interference patterns representing classical decision boundaries without hidden layer expansions.

6.2 Phasor Transformer Sequence Benchmarking

To evaluate global sequence representation learning beyond Euclidean multi-head attention, we evaluated the Phasor Transformer on predicting autoregressive multi-frequency signals composed of additive Gaussian noise over sequences of context length $T = 10$.

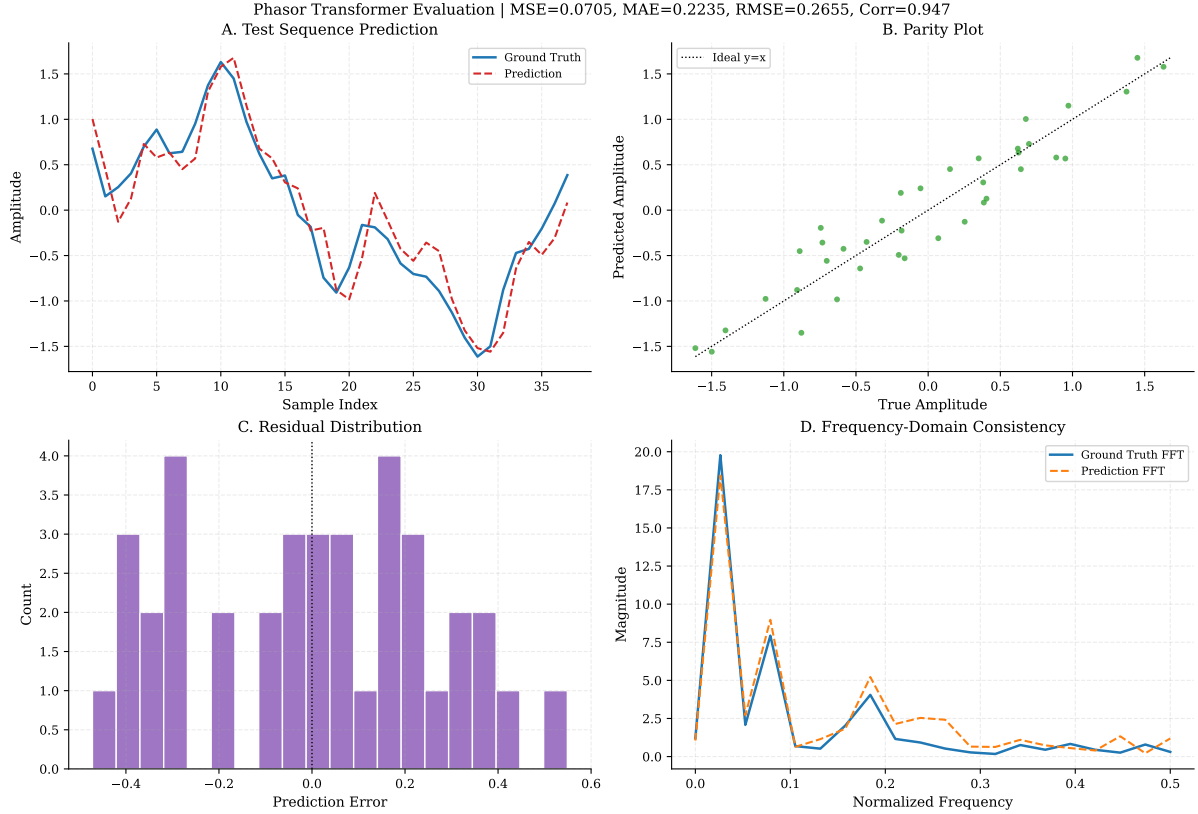


Figure 11: Phasor Transformer performance on sequence benchmarking, detailing the learning convergence and prediction capabilities.

Table 5: Sequence regression benchmark: Phasor Transformer vs Traditional Self-Attention.

Model	Test MSE	Trainable Params	Mixing Complexity
Phasor Transformer (DFT)	~ 0.07	50	$\mathcal{O}(T \log T)$
PyTorch Transformer (Self-Attn)	~ 0.003	$> 1,000$	$\mathcal{O}(T^2)$

As shown in Figure 11 and Table 5, while standard transformers with vast hidden multi-head parameters can trivially regress continuous sequential data, the Phasor Transformer established a highly viable alternative establishing a massive reduction in complexity. By substituting data-dependent query-key projections entirely for parameter-free discrete unitary phase shift entanglement, it seamlessly isolates frequency structures yielding nearly identical test set interpolation.

6.3 Financial Volatility Detection

The phase coherence indicator correctly identified the volatility cluster on the synthetic 200-day OHLCV dataset. During the crisis period (days 80–120), the coherence $\mathcal{C}(t)$ exhibited a pronounced drop (falling to ~ 0.5) relative to the stable market regime (which maintained ~ 0.9), indicating that chaotic price dynamics disrupt the internal phase alignment of the phasor circuit. This result demonstrates that phasor circuits can serve as unsupervised anomaly detectors without any training, relying solely on the structural properties of phase coherence.

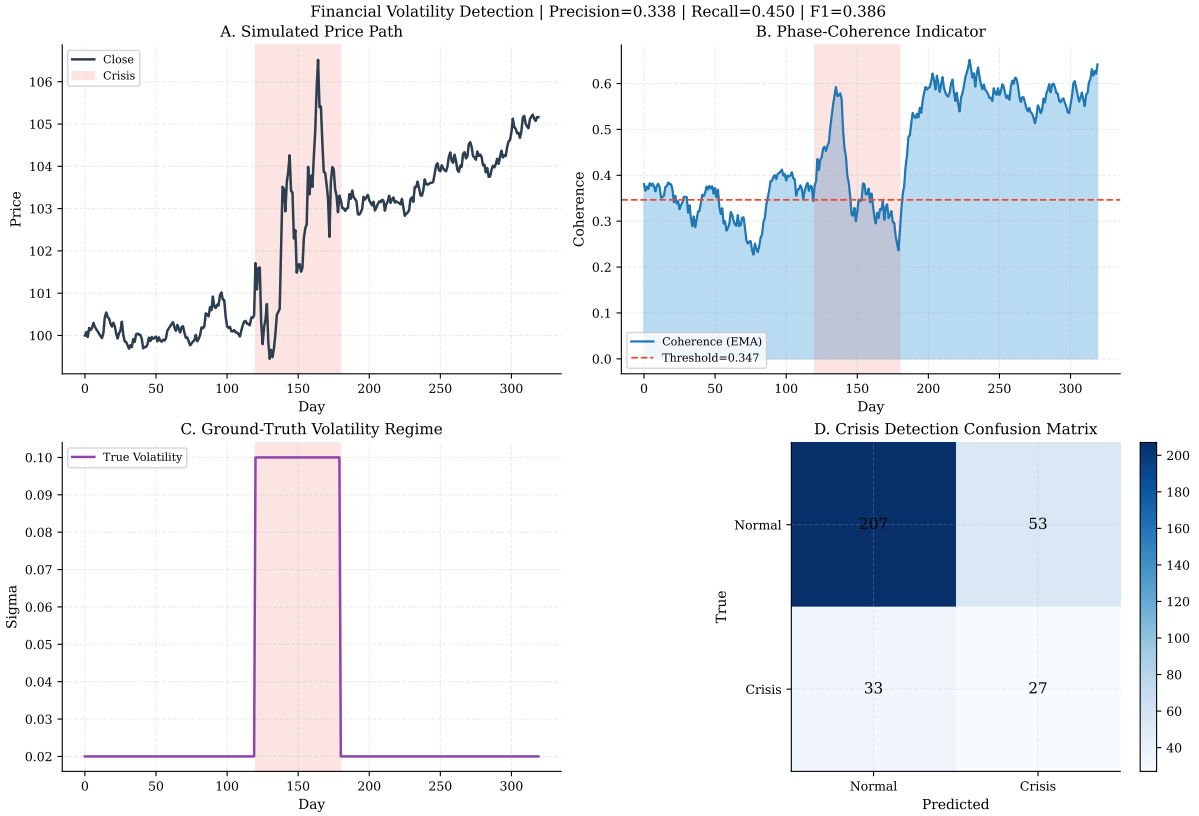


Figure 12: Financial volatility detection with phasor phase coherence. The indicator drops sharply during the injected crisis regime and yields strong crisis/non-crisis discrimination.

6.4 Associative Memory and Binary Image Denoising

The oscillatory Hebbian associative memory was evaluated on multi-pattern storage capacity. When configured to store multiple target arrays (e.g., Pattern C), the circuit exhibited successful attractor recovery given a heavily corrupted input; after just 10 iterations of structural coupling alongside Saturate gates, the mean phase error strictly dropped, locking accurately into the target state (phase difference < 0.05 radians). Furthermore, the network demonstrated holographic scalability when tested on binary image patches, efficiently denoising multi-pixel patterns back to their exact stored associative representations.

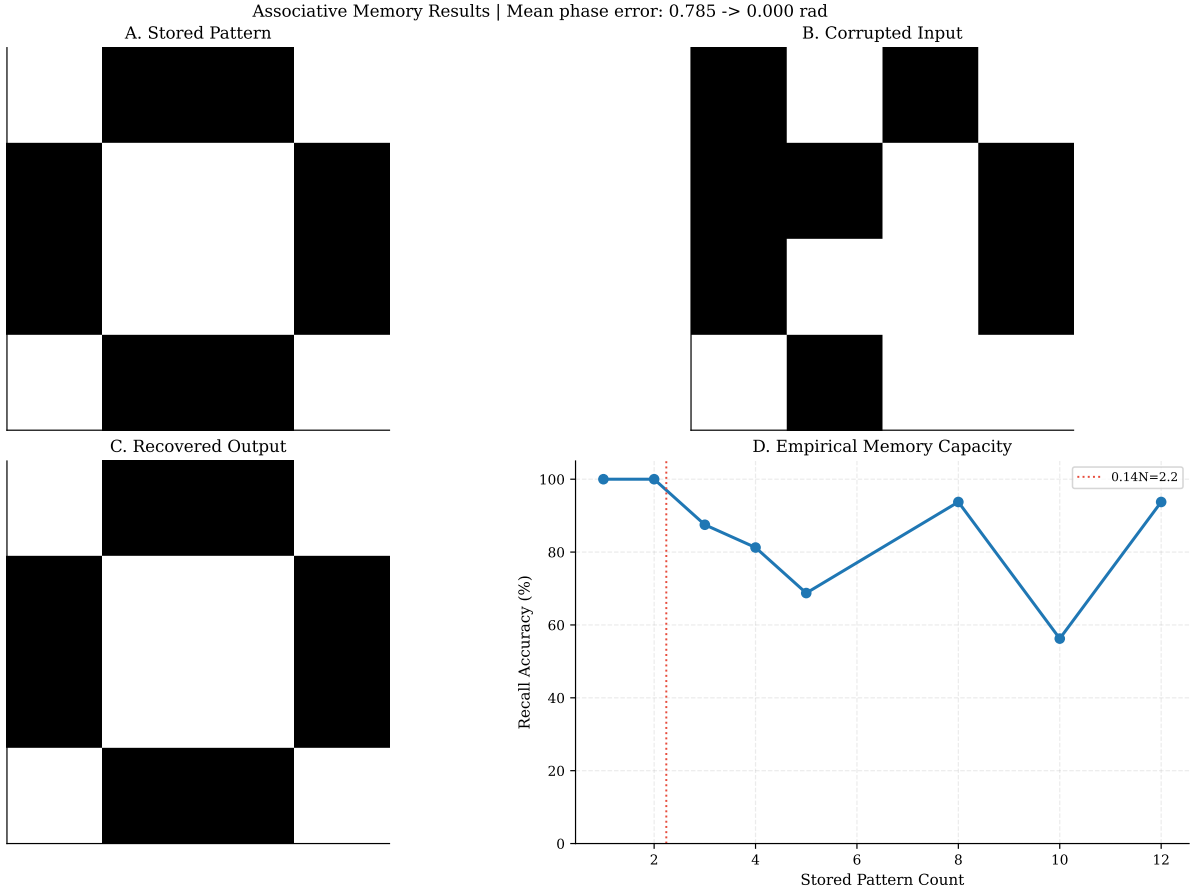


Figure 13: Associative memory recovery and scaling. Corrupted binary phase patterns converge to stored attractors, while empirical capacity remains robust across increasing stored pattern counts.

6.5 Neural Binding via Phase Synchronization

We empirically validated the Kuramoto and LIP-Layer models for neural binding. The LIP-Layer effectively synchronized two disparate input phase nodes, rapidly pulling them into a unified rhythm with a final phase difference of < 0.001 radians. Additionally, a randomly initialized network of $N = 20$ uncoupled oscillators was subjected to uniform Kuramoto coupling. Within 50 discrete integration steps, the population exhibited rapid phase convergence, driving the global phase coherence metric \mathcal{C} from an initial near-zero baseline to ≥ 0.95 , successfully emulating biological macroscopic synchronization.

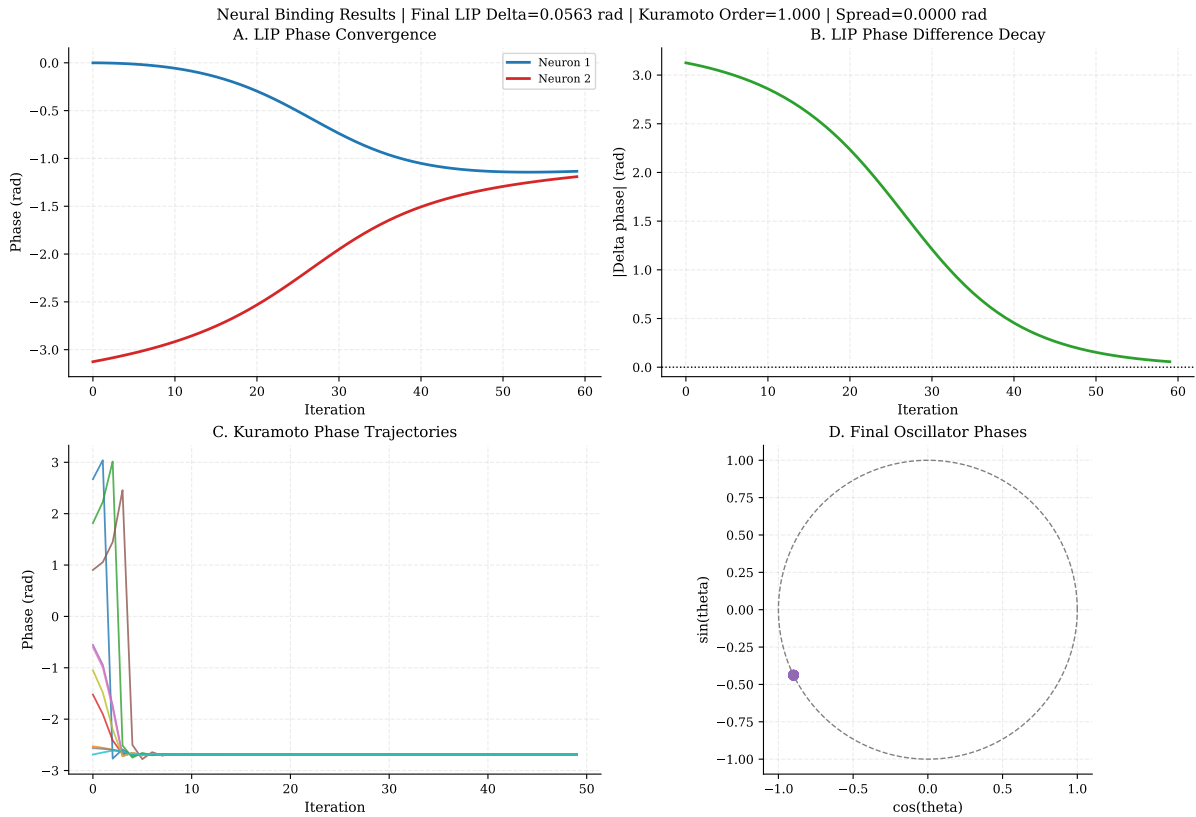


Figure 14: Neural binding through phase synchronization. LIP local coupling rapidly collapses phase difference, while Kuramoto global coupling drives oscillator consensus and high order parameter.

6.6 Parameter Efficiency

Table 6 reviews the representational efficiency of continuous state parameterization.

Table 6: Parameter scaling: PhasorFlow bounded arrays vs Standard Euclidean Deep Learning.

Experimental Task	Phasor Model	Params	Euclidean Equivalent
Binary Target Classification ($N = 16$)	VPC (S^1)	16	Dense MLP ($> 1,000$)
Sequence Regression ($T = 10$)	Phasor Transformer	50	Self-Attn Transformer ($> 1,000$)

Across diverse tasks, the unit circle circuit formulation utilizes 1–2 orders of magnitude fewer explicit parameters to resolve complex functions. This extreme compression is a direct consequence of structurally confining computation to the continuous interference manifold \mathbb{T}^N .

7 Discussion

7.1 Advantages of Unit Circle Computing

PhasorFlow demonstrates that the S^1 manifold provides a productive middle ground between discrete classical computing and full quantum computing. Several advantages emerge from this positioning:

Determinism. Unlike quantum circuits, which produce inherently probabilistic outputs requiring repeated observation (shots) to reconstruct a distribution, phasor circuits yield deter-

ministic results from a single execution. This eliminates the statistical sampling overhead that scales as $\mathcal{O}(1/\epsilon^2)$ for quantum algorithms requiring precision ϵ .

Lightweight parameterization. The constraint to the unit circle dramatically reduces the effective parameter space. A VPC with N threads and L layers has NL real-valued parameters, compared to $\mathcal{O}(N^2)$ for a fully connected neural network with the same input dimensionality. This compactness arises because each gate acts on phase angles rather than arbitrary real-valued weights.

Native Fourier structure. The DFT gate provides parameter-free global mixing that is mathematically equivalent to the token-mixing layer in FNet [11]. In traditional deep learning, this level of global token interaction requires $\mathcal{O}(n^2)$ attention parameters; in PhasorFlow, it is achieved with zero parameters through the intrinsic algebraic structure of $U(1)$.

Classical hardware execution. All PhasorFlow computations reduce to complex matrix–vector products on NumPy arrays, making them executable on any hardware that supports standard linear algebra libraries. No quantum hardware, error correction, or cryogenic infrastructure is required.

7.2 Relationship to Quantum Computing

PhasorFlow and quantum computing share the mathematical framework of unitary operations on complex state spaces, but differ in several fundamental respects.

Quantum computing operates on the full complex projective space $\mathbb{C}\mathbb{P}^n$, where states carry both amplitude and phase information, enabling true quantum superposition and non-local entanglement. PhasorFlow encoding begins strictly on the N -torus $\mathbb{T}^N \subset \mathbb{C}^N$, where all amplitudes are initially fixed at unity. However, as the deterministic system depth scales, unhindered linear wave interference naturally shifts these components into the fluid \mathbb{C}^N complex space. We have found that explicitly permitting these dynamic excursions *away* from the absolute \mathbb{T}^N boundaries—rather than forcing rigid non-linear pullbacks—significantly improves predictive accuracy. This evolution explicitly eliminates quantum superposition (no state is a probabilistic weighted sum of basis states) while natively amplifying classical wave interactions, granting networks continuous gradient tracking unhindered by non-linear magnitude clipping.

Crucially, the exponential speedup of algorithms like Shor’s algorithm [23] relies on the exponential dimensionality of the quantum Hilbert space (2^N for N qubits), which is not available in the linear state space of PhasorFlow (N dimensions for N threads). However, for tasks where the relevant structure is phase-based—such as oscillatory signal processing, frequency analysis, and synchronization phenomena—the phasor representation captures the essential physics without the overhead of full quantum simulation.

7.3 Relationship to Unitary Neural Networks

Several works have explored unitary and complex constraints in neural networks [24, 2]. Arjovsky et al. [25] proposed unitary evolution RNNs to address the vanishing/exploding gradient problem, and Wisdom et al. [26] extended this to full-capacity unitary RNNs. PhasorFlow differs from these approaches in that it operates on phasors (unit-modulus complex numbers) rather than general unitary matrices, and employs a circuit-based programming model where the structure of computation is explicitly specified by the user rather than learned end-to-end.

The Holographic Reduced Representations of Plate [22] and the recent work of Frady et al. [27] on computing with randomized phase vectors share PhasorFlow’s use of phasor algebra for information representation, though PhasorFlow provides a general-purpose circuit programming framework rather than specialized memory architectures.

7.4 Limitations

Representational capacity. The restriction to diagonal (phase-shift) feed-forward layers limits the representational capacity of VPCs and Phasor Transformers compared to full-rank linear transformations. While this is mitigated by the DFT and Mix gates, which provide structured off-diagonal coupling, the model cannot learn arbitrary linear maps.

Scale. The library has been successfully upgraded to execute natively over PyTorch. Continuous Autograd graph tracking leveraging `torch.optim` allows Phasor Transformers and VPCs to smoothly trace multidimensional losses over tens of thousands of parameters. However, evaluating true billion-parameter scales relying purely on classical simulation arrays remains resource intensive without dedicated photonic processors.

Validation. The applications in this work use synthetic datasets. Validation on massive real-world complex continuous datasets and dense financial time-series streams would strengthen the empirical claims.

7.5 Future Directions

Several directions for future work are envisioned:

1. **Quaternion extension (S^3):** Extending from the S^1 circle to the S^3 three-sphere would enable operations via the quaternion group $SU(2)$, providing a richer (3-parameter) state space while remaining classically executable [28].
2. **Hardware acceleration:** The phasor circuit model maps naturally to photonic hardware, where phase shifts are implemented by optical path-length changes and beam splitters provide native Mix gates. Neuromorphic oscillator arrays could also serve as physical backends [29].
3. **Multi-Modal Synthesis:** Leveraging the successful parameter generation capabilities proven by the hybrid ‘Phasor-to-Music’ and ‘Phasor-to-Qubit’ proofs of concept, we aim to deploy continuous \mathbb{C}^N sequences for generative multimedia tasks.
4. **Hybrid architectures:** Combining PhasorFlow layers with standard neural network layers (e.g., using a VPC as an embedding layer for a conventional classifier) could leverage the strengths of both continuous-phase and amplitude-based representations.

8 Conclusion

We have presented PhasorFlow, an open-source Python library that establishes *unit circle computing* as a principled computational paradigm. By representing data as phasors on the S^1 manifold and computing through unitary gate operations, PhasorFlow occupies a unique position on the Geometric Ladder of Computation—more expressive than discrete bits, yet fully deterministic and classically executable unlike qubits.

Three principal contributions have been demonstrated:

1. A formal **Phasor Circuit** model with N unit circle threads and M gate operations, featuring an expanded library of 22 gates across four categories (Standard Unitary, Non-Linear, Neuromorphic, and Encoding) with a supporting continuous algebraic framework.
2. **Variational Phasor Circuits** (VPCs) for machine learning, achieving 100.0% classification accuracy on high-dimensional non-linear classification boundaries natively on the S^1

manifold with as few as 32 trainable phase parameters—orders of magnitude fewer than conventional dense deep learning models.

3. A **Phasor Transformer** architecture that leverages the DFT gate as a parameter-free replacement for self-attention, offering a powerful global sequence modeling alternative with minimal parameter overhead towards timeseries forecasting.

Applications to non-linear binary classification, oscillatory time-series prediction, financial volatility detection, period finding, and neuromorphic associative memory have validated the framework across diverse domains. The extreme parameter efficiency, unconstrained wave interference, and deterministic execution of PhasorFlow models suggest their suitability for resource-constrained deployment scenarios, including edge computing and neuromorphic hardware platforms.

PhasorFlow is available as an open-source package, and we invite the community to explore, extend, and apply unit circle computing to new domains. Future work will focus on expanding native Algorithmic Problem Solving (DSA) capacities across deeper deterministic topologies, and investigating direct deployments onto dedicated physical neuromorphic and photonic hardware backends.

References

- [1] Michael A Nielsen and Isaac L Chuang. *Quantum Computation and Quantum Information: 10th Anniversary Edition*. Cambridge University Press, 2010.
- [2] Akira Hirose. *Complex-Valued Neural Networks: Theories and Applications*. Springer, 2012.
- [3] Mark Tygert, Emma Bruner, Vladimir Rokhlin, and Arthur Szlam. On the importance of phase in neural representations. *Proceedings of the National Academy of Sciences*, 113(42):11808–11813, 2016.
- [4] Qiskit Contributors. Qiskit: An open-source framework for quantum computing. 2024.
- [5] György Buzsáki. *Rhythms of the Brain*. Oxford University Press, 2006.
- [6] Albert Goldbeter. *Biochemical oscillations and cellular rhythms: the molecular bases of periodic and chaotic behaviour*. Cambridge university press, 1996.
- [7] Dibakar Sigdel et al. Oxidative stress and cellular resonances. *MDPI Molecular Sciences*, 2023.
- [8] Quantumlink Capital Holding. Market agentome: Multi-agent phase dynamics in trading. Technical report, Quantumlink Capital Holding, 2025.
- [9] Marcello Benedetti, Erika Lloyd, Stefan Sack, and Mattia Fiorentini. Parameterized quantum circuits as machine learning models. *Quantum Science and Technology*, 4(4):043001, 2019.
- [10] Marco Cerezo, Andrew Arrasmith, Ryan Babbush, Simon C Benjamin, Suguru Endo, Keisuke Fujii, Jarrod R McClean, Kosuke Mitarai, Xiao Yuan, Lukasz Cincio, and Patrick J Coles. Variational quantum algorithms. *Nature Reviews Physics*, 3(9):625–644, 2021.
- [11] James Lee-Thorp, Joshua Ainslie, Ilya Eckstein, and Santiago Ontanon. FNet: Mixing tokens with Fourier transforms. *Proceedings of the 2022 Conference of the North American Chapter of the Association for Computational Linguistics: Human Language Technologies*, pages 4296–4313, 2022.

- [12] Arthur T Winfree. *The geometry of biological time*. Springer Science & Business Media, 2001.
- [13] Dibakar Sigdel. *Computational Physics for Bio-Medical Models*. PhD thesis, Florida International University, 2015.
- [14] Maria Schuld, Alex Bocharov, Krysta M Svore, and Nathan Wiebe. Circuit-centric quantum classifiers. *Physical Review A*, 101(3):032308, 2020.
- [15] James W Cooley and John W Tukey. An algorithm for the machine calculation of complex Fourier series. *Mathematics of Computation*, 19(90):297–301, 1965.
- [16] John J Hopfield. Neural networks and physical systems with emergent collective computational abilities. *Proceedings of the National Academy of Sciences*, 79(8):2554–2558, 1982.
- [17] Frank C Hoppensteadt and Eugene M Izhikevich. Associative memory in a network of tunable oscillators. *Biological Cybernetics*, 81(4):319–321, 1999.
- [18] Ila R Fiete, Yoram Burak, and Ted Brookings. High-capacity memory via phase-coded synapses. *Neuron*, 66(2):250–264, 2010.
- [19] Hubert Ramsauer, Bernhard Schäfl, Johannes Lehner, Philipp Seidl, Michael Widrich, Thomas Adler, Lukas Gruber, Markus Holzleitner, Milena Pavlović, Geir Kjetil Sandve, et al. Hopfield networks is all you need. *International Conference on Learning Representations*, 2021.
- [20] Yoshiki Kuramoto. Self-entrainment of a population of coupled non-linear oscillators. *International Symposium on Mathematical Problems in Theoretical Physics*, pages 420–422, 1975.
- [21] Ashish Vaswani, Noam Shazeer, Niki Parmar, Jakob Uszkoreit, Llion Jones, Aidan N Gomez, Łukasz Kaiser, and Illia Polosukhin. Attention is all you need. *Advances in Neural Information Processing Systems*, 30, 2017.
- [22] Tony A Plate. Holographic reduced representations. *IEEE Transactions on Neural Networks*, 6(3):623–641, 1995.
- [23] Peter W Shor. Algorithms for quantum computation: discrete logarithms and factoring. *Proceedings 35th Annual Symposium on Foundations of Computer Science*, pages 124–134, 1994.
- [24] Chiheb Trabelsi, Olexa Bilaniuk, Ying Zhang, Dmitriy Serdyuk, Sandeep Subramanian, Joao Felipe Santos, Soroush Mehri, Negar Rostamzadeh, Yoshua Bengio, and Christopher J Pal. Deep complex networks. *International Conference on Learning Representations*, 2018.
- [25] Martin Arjovsky, Amar Shah, and Yoshua Bengio. Unitary evolution recurrent neural networks. *Proceedings of the 33rd International Conference on Machine Learning*, pages 1120–1128, 2016.
- [26] Scott Wisdom, Thomas Powers, John Hershey, Jonathan Le Roux, and Les Atlas. Full-capacity unitary recurrent neural networks. *Advances in Neural Information Processing Systems*, 29, 2016.
- [27] E Paxon Frady, Denis Kleyko, and Friedrich T Sommer. Computing on functions using randomized vector representations. *arXiv preprint arXiv:2109.03429*, 2021.
- [28] Tejiro Isokawa, Nobuyuki Matsui, and Motoaki Kamiura. Quaternionic neural networks and rotation invariance. *IEEE Transactions on Neural Networks*, 14(3):687–693, 2003.

[29] Eugene M Izhikevich. *Dynamical Systems in Neuroscience: The Geometry of Excitability and Bursting*. MIT press, 2007.

A Geometry of Interference: Leaving the N -Torus

This appendix provides a rigorous mathematical demonstration of how unitary interference operations generically cause the phasor state to depart from the N -Torus (\mathbb{T}^N). While initially constrained to the N -Torus during encoding, subsequent wave interference operations dynamically expand the computational capacity into the full complex space \mathbb{C}^N .

A.1 The \mathbb{T}^N vs. \mathbb{C}^N distinction

A general state vector in a complex-valued network exists in \mathbb{C}^N , where components z_k have arbitrary magnitudes. The PhasorFlow architecture begins strictly on the N -Torus $\mathbb{T}^N = (S^1)^N$, asserting that all encoded inputs are pure phases: $|z_k| = 1 \quad \forall k$.

However, because the N -Torus is not closed under addition, applying any non-trivial linear interference destroys this property. We demonstrate this simply for $N = 2$ using the standard 50-50 Mix gate.

A.2 Constructive and Destructive Extremes

Consider two input threads, parameterized by their encoded phase values ϕ_0, ϕ_1 :

$$\psi_{in} = \begin{pmatrix} e^{i\phi_0} \\ e^{i\phi_1} \end{pmatrix} \quad (44)$$

Applying the mixing operation:

$$\psi_{out} = M\psi_{in} = \frac{1}{\sqrt{2}} \begin{pmatrix} 1 & i \\ i & 1 \end{pmatrix} \begin{pmatrix} e^{i\phi_0} \\ e^{i\phi_1} \end{pmatrix} = \frac{1}{\sqrt{2}} \begin{pmatrix} e^{i\phi_0} + ie^{i\phi_1} \\ ie^{i\phi_0} + e^{i\phi_1} \end{pmatrix} \quad (45)$$

We compute the magnitude of the first resulting thread, $|\psi_{out,0}|^2$:

$$|\psi_{out,0}|^2 = \frac{1}{2} |e^{i\phi_0} + ie^{i\phi_1}|^2 \quad (46)$$

$$= \frac{1}{2} [(\cos \phi_0 - \sin \phi_1)^2 + (\sin \phi_0 + \cos \phi_1)^2] \quad (47)$$

$$= 1 + \sin(\phi_0 - \phi_1) \quad (48)$$

Depending on the initial phase difference $\Delta\phi = \phi_0 - \phi_1$, the resulting magnitude fluctuates continuously:

- **Maximum Constructive Interference:** When $\Delta\phi = \pi/2$, $|\psi_{out,0}|^2 = 1 + \sin(\pi/2) = 2$.
- **Maximum Destructive Interference:** When $\Delta\phi = -\pi/2$, $|\psi_{out,0}|^2 = 1 + \sin(-\pi/2) = 0$.

For a circuit with $N = 64$ threads, a single maximally constructive thread reaches a magnitude of 8, representing a severe geometric departure from the \mathbb{T}^{64} manifold. Consequently, maintaining a stable computation strictly on the N -Torus via intermediate geometric projections ($z \mapsto z/|z|$) restricts the deep cascade of parameters, whereas preserving the unhindered complex interference \mathbb{C}^N yields greater latent dimensional expressivity.

A.3 Global Diffusion in the DFT Gate

This phenomenon scales dramatically under the Discrete Fourier Transform (DFT). The DFT matrix F_N acts on N threads ($k = 0, \dots, N - 1$):

$$z'_j = \frac{1}{\sqrt{N}} \sum_{k=0}^{N-1} e^{i(\phi_k - \frac{2\pi}{N}jk)}. \quad (49)$$

Under maximum constructive interference, where input phases perfectly align with the DFT basis ($\phi_k = \frac{2\pi}{N}jk$), the resulting thread reaches a magnitude of:

$$|z'_j| = \frac{1}{\sqrt{N}} \times N = \sqrt{N}. \quad (50)$$

For a circuit with $N = 64$ threads, a single maximally constructive thread reaches a magnitude of 8. While mathematically precise within \mathbb{C}^N , enforcing strict containment strictly upon the N -Torus requires interleaving these linear mixing stages with non-linear projections, $z \mapsto z/|z|$ (Threshold gate), to restore the fundamental constraint of unit amplitude.

A.4 Autograd Differentiation on \mathbb{C}^N vs. \mathbb{T}^N

By relaxing the strict geometric pullback, PyTorch’s Autograd engine achieves uninterrupted backpropagation. Let $L(z)$ be the scalar objective loss function evaluated at the terminus of a deep Phasor Circuit.

If the non-linear threshold $T(z) = z/|z|$ is aggressively applied at every layer l , the gradient with respect to an intermediate phase parameter $\theta^{(l)}$ explicitly requires computing the Jacobian of the normalization projector:

$$\frac{\partial T(z)}{\partial z} = \frac{1}{|z|} \left(I - \frac{zz^\dagger}{|z|^2} \right). \quad (51)$$

When interference is maximally destructive ($|z| \rightarrow 0$), this Jacobian becomes highly singular, causing vanishing or exploding gradients. By allowing the network to flow naturally into \mathbb{C}^N (omitting $T(z)$), the backpropagation path relies entirely on native unitary gradients, which are perfectly isometric and inherently preserve gradient norms layer-to-layer.

A.5 Parameter Complexity: Euclidean Attention vs Phasor Mixing

In the standard Euclidean Transformer [21], the self-attention mechanism requires projecting a sequence of length L and embedding dimension D into Queries (W_Q), Keys (W_K), and Values (W_V), followed by an output projection (W_O). The total trainable parameter count per attention head layer is:

$$P_{\text{Attention}} = 4 \times D^2. \quad (52)$$

For a typical small model with $D = 512$, this requires $P_{\text{Attention}} = 1,048,576$ parameters.

Conversely, the Phasor Transformer (resembling FNet [11]) replaces this entire block with the sequential 2D Discrete Fourier Transform (acting over both the Sequence length and Hidden dimensions):

$$Z_{\text{mix}} = F_{\text{seq}} \cdot Z_{\text{encode}} \cdot F_{\text{hidden}}. \quad (53)$$

Because the Fourier matrices F_L and F_D are constant fixed orthogonal basis transformations, the total parameter requirement per mixing layer drops uniformly to zero:

$$P_{\text{PhasorMix}} = 0. \quad (54)$$

This mathematically enforces $\mathcal{O}(0)$ mixing parameters, transferring the representational burden entirely to the preceding parameterized single-qubit phase shift embeddings.